J Solid State Electrochem (2010) 14:271–277
DOI 10.1007/s10008-009-0820-7

ORIGINAL PAPER

A new strategy for fabrication Fe_2O_3/SiO_2 composite coatings on the Ti substrate

Arūnas Jagminas · Rimas Ragalevičius · Kestutis Mažeika · Jonas Reklaitis · Vitalija Jasulaitienė · Algis Selskis · Dalis Baltrūnas

Received: 16 November 2008 / Revised: 20 January 2009 / Accepted: 27 February 2009 / Published online: 13 March 2009

Abstract We report here on the synthesis of homogenous, well-adherent composite film of Fe_2O_3/SiO_2, up to 7 μm thick, on the titanium substrate by anodic treatment optimized for an aqueous suspension of $K_2O{\cdot}SiO_2$ and Fe_2O_3 powder under galvanostatic conditions. The end products were characterized by scanning electron microscopy, energy-dispersive X-ray, X-ray powder diffractometry, X-ray photoelectron spectroscopy, and Mössbauer spectroscopy, concluding that the formation of composite coating at the SiO_2 to Fe_2O_3 ratio of approximately 1:1 proceeds just after formation of a thin TiO_2 layer with Fe_2O_3 particle inclusions without transformations via an electrophoresis deposition of negatively charged Fe_2O_3 species enveloped by silica ions.

Keywords Fe_2O_3/SiO_2 composites · Electrophoresis deposition · Anodizing · Titanium

Introduction

Materials based on the assembly of sub micrometer and nanometer-scaled particles of iron oxides such as magnetite (Fe_3O_4), hematite (α-Fe_2O_3), maghemite (γ-Fe_2O_3), goethite (α-FeOOH), and umangite (β-FeOOH) have been reported as promising candidates in the production of gas sensors, photocatalysts, and, especially, hard and soft magnets [1–4]. These materials can be fabricated by chemical vapor condensation [5–7] and decomposition [8], electrodeposition in the manholes of various templates [9], electrophoresis deposition [10], sol–gel approach [11], thermally [12], and chemically [13]. Currently, attention is focused on the films of the spinel-type iron oxide sub-micrometer-scaled and nanometer-scaled particles of Fe_3O_4 and γ-Fe_2O_3 exhibiting higher coercitivity than their bulk parents [14], depending on the shape of the end products and the processing conditions [15]. To prevent agglomeration and magnetic separation of particles, they are frequently immobilized onto supporting surfaces and frameworks such as zeolites [16], glass beads [17], porous silica [18], and alumina [19].

Hematite (α-Fe_2O_3) is the most stable iron oxide under ambient conditions with a band gap of 2.1 eV. Traditionally, α-Fe_2O_3 is used as catalyst [20], gas-sensing [21], and solar energy conversion material [22]. In recent years, the unusual magnetic properties of hematite particles have also been reported [23, 24]. It is known that iron oxides can be directly coated with amorphous silica because the surface of iron oxides has strong affinity towards silica [25]. Due to this, a wide range of different conditions have been reported for obtaining iron oxide particles in silica matrix [26–28].

The anodizing of valve metals such as aluminum and titanium in slurry solutions (suspensions) under galvanostatic conditions is a rather new field of micro-arc oxidation [29]. The addition of different powdered materials such as oxides, nitrides, borides, carbides, etc. into electrolytes allows one to change the composition and properties of obtained coatings. However, these processes have not been sufficiently studied yet and variables in composition of slurry solutions can give unexpected results.

In this study, we report on a new strategy for the formation of α-Fe_2O_3/SiO_2 composite coating via an electrophoresis deposition in the anodizing bath of the titanium substrate. To the best of our knowledge, there have been no similar studies of the combined anodizing/plating process resulting in the formation of composite coating from iron oxide particles and

A. Jagminas (✉) · R. Ragalevičius · V. Jasulaitienė · A. Selskis
Institute of Chemistry,
A. Goštauto 9, 01108 Vilnius, Lithuania
e-mail: jagmin@ktl.mii.lt

K. Mažeika · J. Reklaitis · D. Baltrūnas
Institute of Physics,
Savanorių 231, 02300 Vilnius, Lithuania

amorphous silica oxide on TiO_2. Additionally, we also try to understand the origin of the processes taking place on the Ti anode surface.

Experimental

Materials

Titanium foil, 100 μm thick and 99.7 at.% purity, purchased from Aldrich was used as a raw material for fabrication of rectangular (10×10 mm^2) samples. Prior to use, the surface of specimens was degreased in acetone and distilled water, then chemically cleaned in 15% hydrofluoric acid solution at room temperature for 60 s, rinsed thoroughly, and dried in an air stream. The chemicals used in this study were: 40% potassium silicate solution at the K_2O to SiO_2 molar ratio of 1:3.1 purchased from Askania AB (Sweeden), Fe_2O_3 powder of analytical grade (Russia), and water from Milli-Q water system.

Fabrication

Fe_2O_3 powder was used as received, without any cleaning procedure before experiments. The mean size of the particles, determined from the scanning electron microscope images, was approximately 0.1 μm, but the grain size varied from 0.03 to 0.15 μm.

To wet and suspend uniformly Fe_2O_3 particles in the potassium silicate solution, the powder was immersed into the bath and then stirred for 1 h before initiation of the process. The coatings were formed with continuous stirring of the working solution at the magnetic stirrer (3.0 g) turning velocity of 175 circle/min in a 0.25-dm^3 double-walled cylindrical glass cell through which a thermostated water was pumped to maintain the bath temperature at 293±1 K. Two stainless steel sheets, of 4×13-cm size, spaced ~70 mm apart, were used as the cathode. A working Ti electrode was completely immersed in the central part of the cell. A direct current supply (voltage up to 900 V, current up to 0.5 A) under constant current density (j_a) control was used in this study. After coating, lasting for up to 1 h, specimens were rinsed with water and dried in an air stream for morphological, phase, and compositional analysis. The control dip coating experiment was done in the same vigorous stirred slurry solution for 15 min without an applied electric field.

Characterization methods

The average thickness of the resulting coatings was determined using an optical microscope Neophot 2 from ten measurements on both sides of the cross-sectioned samples encapsulated in the epoxy tablet before cutting and mechanical polishing.

The phase composition of as-grown products was investigated using an X-ray diffractometer D8 (Bruker AXS, Germany) equipped with a Göbel mirror for CuK_α radiation. In these measurements, the scanning step of 0.02°/s in the 2Θ range from 20° to 70° was used.

A scanning electron microscope (SEM, model EVO 50 EVP) equipped with the energy-dispersive X-ray (EDX) spectroscope (Oxford Instruments) was used for observations and elemental analysis of suspension species and as-formed coatings.

Mössbauer spectra (MS) of iron oxide powder and composite coatings were recorded using a constant acceleration mode in the spectrometer (Wissenschaftliche Elektronik GMBH) with a source of ^{57}Co in rhodium. The line width (full width at half-maximum, FWHM) obtained for a α-Fe 25-μm-thick foil, as reference, was approximately 0.28 mm·s^1 at ambient temperature. Experimental spectra were fitted with Lorentzian lines using the least-squares method. All measurements were performed at least in duplicate.

The elemental analysis of the layers grown on the titanium surface at initial stages of the process was performed by X-ray photoelectron spectroscopy (XPS) using a spectrometer ESCALAB-MK 11, UK. A double anode with AlK_α line radiation whose energy was 1486.6 eV and power 300 W (15 kW, 20 mA) was used as the excitation source of photoelectrons. Spectra were recorded in the energy ranges of Ti 2p, Si 2p, O 1s, Fe 2p, and K 2p peaks. The energy scale of the spectrometer was calibrated using the Cu $2p_{3/2}$ peak at 932.4±0.1 eV, Ag $3d_{5/2}$ peak at 368.0±0.1 eV, and Au $4f_{7/2}$ peak at 83.8±0.1 eV. The pressure in the UHV analyzer chamber was maintained at 1.33×10^{-7} Pa. Spectra for every element were recorded three to five times and the data obtained were averaged and compared with standards [30]. The amount of each element was calculated from the integral areas of the photoelectron peaks, their sensitivity factors being taken from the operating instructions of the equipment used. A Shirley background subtraction was carried out for all XPS core level spectra. The spectra were then fitted with Gaussian-type functions. The values of FWHM were maintained between 1.5 and 1.7 eV.

To analyze the depth distribution of elements, the specimens were etched in a preparation chamber at 5×10^{-3} Pa by sputtering argon ions with 2 keV at a current density of ~50 μA cm^{-2} for up to 60 s.

Results and discussion

$K_2O{\cdot}SiO_2$ solutions

Typical voltage–time plots recorded for the Ti anode in the optimized solution of liquid glass at the constant current density of 5.0 and 10 A dm^{-2} are shown in Fig. 1. One can

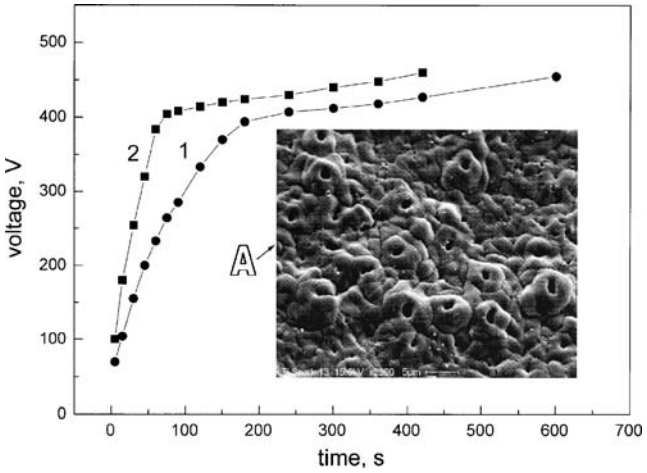

Fig. 1 Voltage–time plots for electrolytic oxidation of titanium in alkaline solution containing 12.5 g dm^{-3} $K_2O{\cdot}SiO_2$ (molar ratio 1:3.1) at the constant current density: (*1*) 5.0; (*2*) 10.0 A dm^{-2}. Inset *A* presents the typical surface morphology of obtained coatings

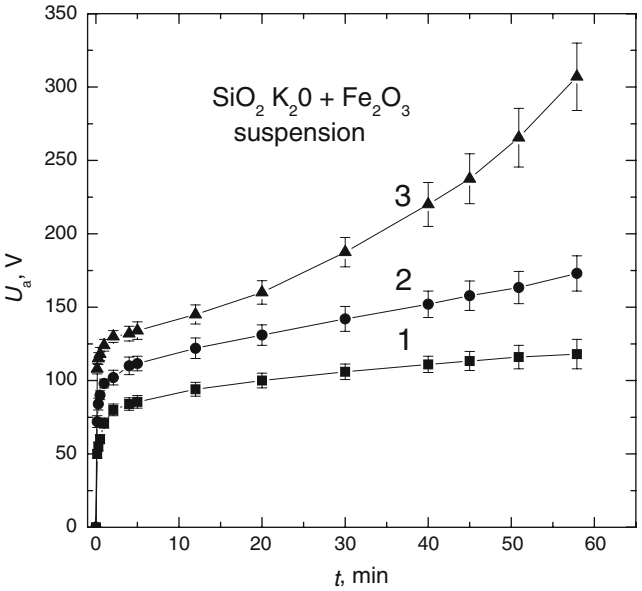

Fig. 2 Voltage–time variations during galvanostatic treatment of titanium anode in a suspension of 12.5 g dm^{-3} $K_2O{\cdot}SiO_2$ (molar ratio 1:3.1) and 5 g dm^{-3} Fe_2O_3 powder at j_a: (*1*) 2; (*2*) 5; (*3*) 10 A dm^{-2}

see that the voltage during oxidation already exceeds the vicinity of 400 V after approximately 1 to 3 min. The most rapid rise of voltage (U_a) proceeds at ~6.5 to 8.0 V s^{-1} rate ($\partial U_a/\partial t$) during the first 15 to 17 s. With continuing treatment and further increasing voltage at a decreasing rate, the anode is enshrouded by the continuous plasma luminescent sparks, accompanied by a low-frequency acoustic emission and $\partial U_a/\partial t$ decreases down to approximately 0.14–0.15 V s^{-1}. It was noted that the first sparks in this solution appeared at around 390 V. The architecture of resulting light gray coatings can be viewed as typical of plasma electrolytic oxidation products (see inset in Fig. 1).

An XPS scan for the specimen anodized at 5.0 A dm^{-2} for 20 min indicated the elements of Ti, Si, O, and some amounts of K. Chemical state analysis indicated the coating composed of Ti^{4+} and Si^{4+}, both bonded with oxygen, like in forms of TiO_2 and SiO_2, respectively, with a negligible content (0.2–0.7 at.%) of K_2O. Furthermore, the XPS depth profiling studies showed a significant increase in TiO_2 from the top (10–15 at%) to the bulk, as expected.

Fe_2O_3-containig suspensions

Typical voltage–time plots recorded for the Ti anode in the Fe_2O_3 powder-containing liquid glass slurry solution under galvanostatic conditions are presented in Fig. 2. As it is seen, a linear growth of U_a observed at the beginning of this process even after 30–60 s slows down, providing later approximately the same U_a growth rate depending on the current density, j_a, value. The increase in j_a results the increase of $\partial U_a/\partial t$ and also determines the maximum U_a value which can be attained during the film growth. Thus, the U_a value, up to approximately 300 V, can be reached during 1-h treatment of the specimen at j_a 10 A dm^{-2} if the solution of optimized composition (12.5 $K_2O{\cdot}SiO_2$, 5 g dm^{-3} Fe_2O_3; pH 11.0) is used. It is noteworthy that any sparks cannot be observed in this case for all processing time. The major parameters determining the behavior of the Ti anode in this suspension are the current density and the concentration of components. The increase in the concentration of liquid glass ($c_{K_2O{\cdot}SiO_2}$) leads to an obvious decrease in the U_a value and the rate of coating growth, while the decrease in $c_{K_2O{\cdot}SiO_2}$—to non-uniform growth under the sparking conditions.

Figure 3 shows the typical SEM top (a, b) and cross-sectional (c) view of the final products fabricated during this process under the optimized conditions for different time laps. From these images, it was concluded that densely packed coating of the thickness of 6–7 μm per hour can be successfully fabricated on the surface of Ti electrode at 10 A dm^{-2}. This brick red coating was found to be well adherent to the substrate and finely grained, although the prolonged processing at high j_a, approximately 10 A dm^{-2}, results in the formation of a ragged coating (see Fig. 3c). It was observed that the morphology of coatings consisted of spherical aggregates of variable size, ≤0.1 μm in diameter, which were composed of nanometer-sized primary species. As is also seen, some of the spherical particles are agglomerated into larger ones of different shapes and sizes up to approximately 0.5 μm.

The composition of coatings

The deposited coatings were further analyzed using X-ray powder diffractometry (XRD) and EDX. In the XRD pattern (Fig. 4), all peaks were indexed to crystalline phase

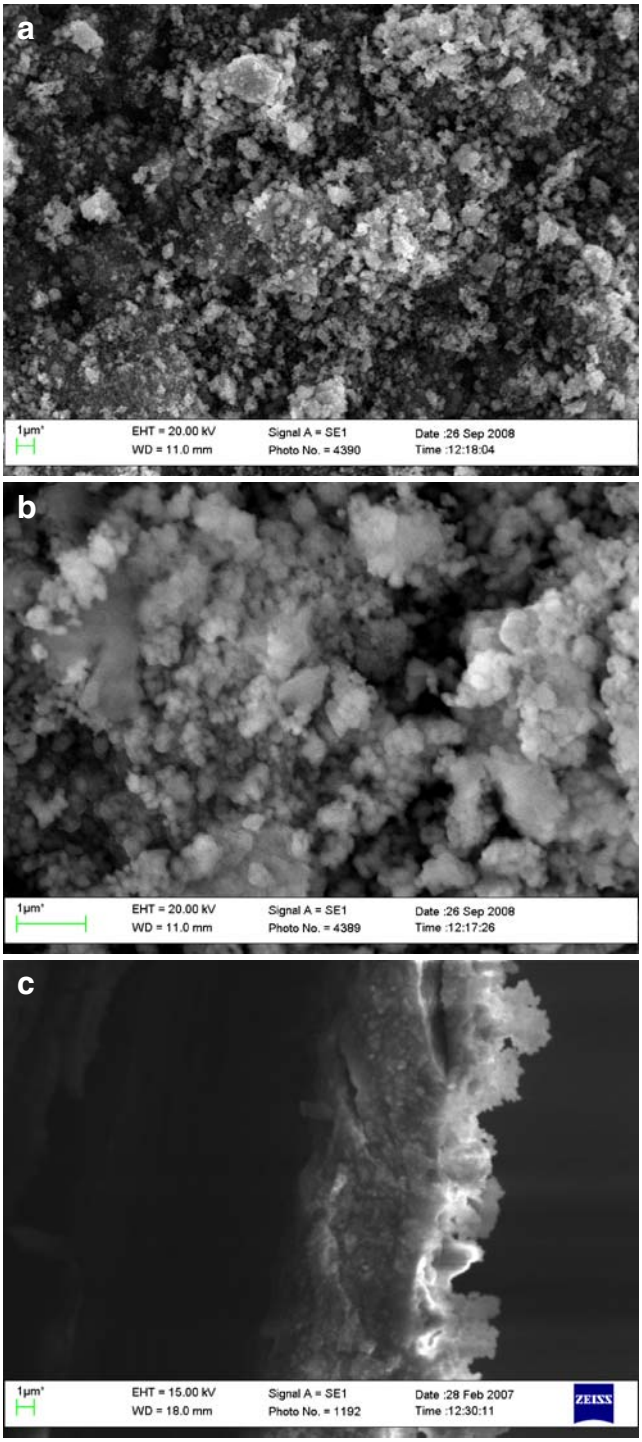

Fig. 3 Top side (**a**, **b**) and cross-sectional (**c**) SEM images of the Ti substrate following the anodic treatment in the same solution as in Fig. 2 at j_a 10 A dm^{-2} for: 5 (**a**), 25 (**b**), and 50 min (**c**)

of α-Fe_2O_3. The intensities of diffraction peaks in the XRD spectrum were found to correlate well with the relative intensities of α-Fe_2O_3 standard (JCPDS card no. 89-2810). No obvious peaks attributed to crystalline phases of TiO_2 were detected. The results obtained by analyzing both sides of the film using EDX are presented in Table 1. From these

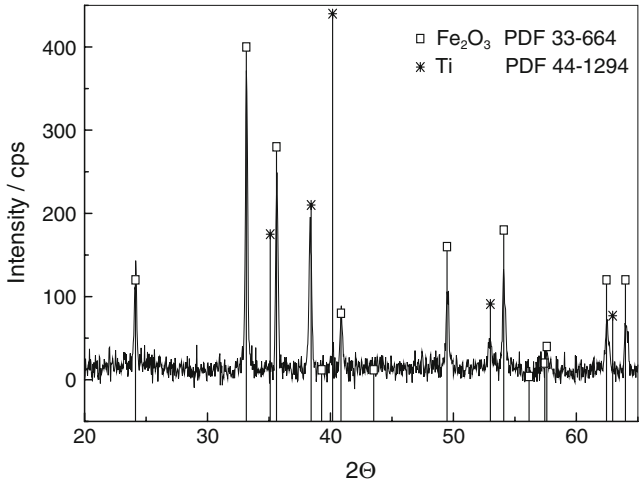

Fig. 4 Typical XRD patterns of as-grown coating

results, one can conclude that this film is mainly composed of Fe_2O_3 and SiO_2 with a marginal content of Ti and K elements incorporated most likely in their amorphous oxide phases. Somewhat larger content of Ti detected from the coating/Ti interface side probably could be related to the formation of a thin intermediate layer of TiO_2, since a sharp increase in the bath voltage up to 100–150 V at the onset of processing can be related only to the anodizing of the Ti substrate which probably took place before the deposition of composite from Fe_2O_3 crystallites and amorphous SiO_2.

The composition of Fe_2O_3 powder used in the preparation of suspensions and the coatings obtained was further analyzed using Mössbauer spectroscopy (MS). The MS spectrum recorded by analyzing Fe_2O_3 powder is shown in Fig. 5a. It can be seen that this spectrum can be well fitted with a sextet with the hyperfine magnetic field of 51.8 T, demonstrating antiferomagnetic features of crystallites of pure hematite (α-Fe_2O_3) phase. We have observed in this setup that the MS spectrum of coatings, fabricated under conditions of this study, is similar to the spectrum of Fe_2O_3 powder (see Fig. 5b) and can also be analyzed using one sextet for hematite implying any compositional or phase transformations of the particles used during the deposition at a high electric field. However, in this case, a single Lorenzian line is needed to account for paramagnetic component in the central

Table 1 EDX results obtained by analyzing the top and back side of the film grown onto Ti surface by anodization in an aqueous suspension of 12.5 g dm^{-3} SiO_2 K_2O and 5 g dm^{-3} Fe_2O_3 powder at j_a 10 A dm^{-2} and room temperature for 50 min

Analysis place	The content of elements (at.%)				
	Fe	O	Si	Ti	K
Top side	19.54	64.15	15.71	0.32	0.29
Back side	15.95	66.58	14.68	2.49	0.31

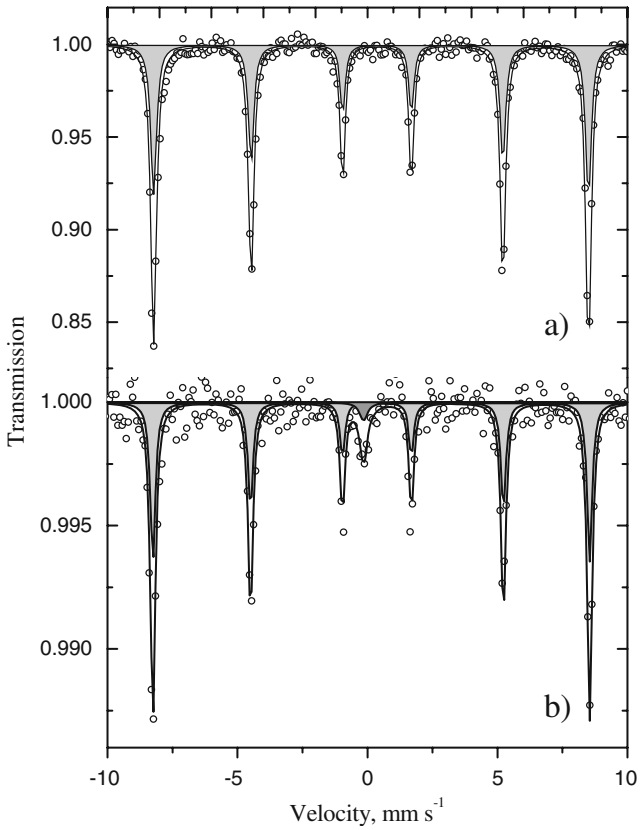

Fig. 5 Mössbauer spectrum (*MS*) of Fe_2O_3 powder used in this study (**a**) and MS of the composite coating formed on the Ti surface in the same slurry solution as in Fig. 2 at j_{ac} 10 A dm^{-2} for 30 min (**b**)

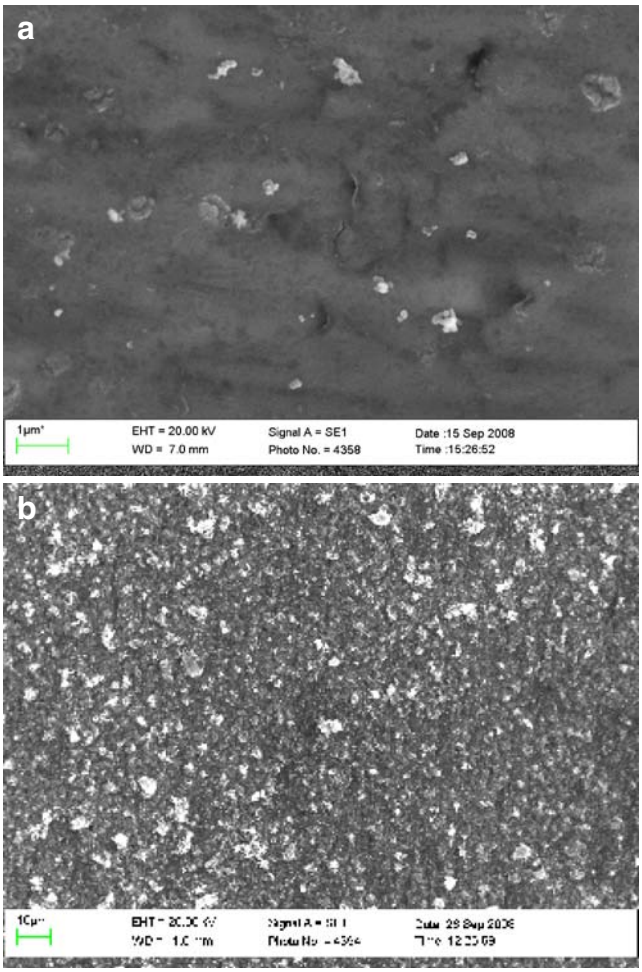

Fig. 6 Typical top side SEM view of the Ti surface at initial stages of anodic treatment in the suspension as in Fig. 2 at 5 A dm^{-2} for 5 to 15 s (**a**) and after 2 min (**b**)

part of the spectrum which cannot be clearly attributed to one or another iron compound. From the analysis of the isomer shift of this singlet, equal to δ=0.04±0.03 mm s^{-1}, we attributed it to Fe atoms in the Ti substrate.

Initial stages of the process

In order to understand the mechanism of formation the Fe_2O_3/SiO_2 composite coatings, the time-dependent composition evolution for layers grown at initial stages was studied carefully by SEM and XPS. In this setup, we have found that in contrast to the behavior of the Ti electrode in Fe_2O_3-free solution, the same anodic treatment in the suspension just after first 5 s results in the formation of colored films. At 5 A dm^{-2}, the color of Ti surface changes in a sequence: gray (2–4 s); light greenish (5–8 s); light yellow (10–13 s); reddish (15–20 s). Furthermore, both SEM and XPS depth profiling studies indicated that Fe_2O_3 particles are dispersed throughout the TiO_2 layer at approximately similar content of about <1.0 at.%. A typical top view of the SEM image of Ti surface after anodic treatment in slurry solution at 5 A dm^{-2} during the first 5 to 15 s is shown in Fig. 6a, while Fig. 6b demonstrates the morphology of the surface just at the onset of composite coating formation. In the case of short-term treatment, the SEM image indicates the randomly distributed inclusions of Fe_2O_3 spherical species (white spots) in a titania film. Approximately the same amount of Fe, detected by XPS depth profiling analysis, allowed us to hypothesize that Fe_2O_3 species were attached to the surface of electrode at the onset of the process. With further processing, the amount of attached species remained approximately the same until the electrode attained the potential drop quite large to provoke the spontaneous deposition of negatively charged species. It was accompanied by an obvious decrease of $\partial U_a/\partial t$ growth slope starting at the bath voltages from 75 to 125 V depending on the current density applied.

The control experiment was done in the same stirred slurry solution for 15 min without an applied electric field. In this case, however, only a small amount of adsorbed species has been observed both onto the Ti and pre-anodized (in the same Fe_2O_3-free solution at 5 A dm^{-2} until the bath of voltage 200 V was attained) Ti surfaces after sonication and rinsing. These results have indicated that in contrast to extremely

small particles [31], Brownian motion of much larger Fe_2O_3 species did not lead to the numerous adsorptions and formation of composite coating in our experiments.

Discussion

Based on the results obtained, the following interpretation of these phenomena can be presented.

The electrochemical treatment of Ti in the alkaline solution of liquid glass, with $K_2O{\cdot}SiO_2$ molar ratio 1:3.1 and pH close to 11 under constant current density control, results in the formation of typical plasma electrolytic oxidation coatings [32]. On the contrary, the same procedure in the same solution containing Fe_2O_3 sub-micrometer-scaled particles leads to the formation of thick composite coatings mainly of the same α-Fe_2O_3 crystalline particles and amorphous SiO_2 at approximately 1:1 content by electrophoresis deposition, preventing a sharp rise in the bath voltage and micro-arc anodizing of Ti. It is likely that for Fe_2O_3 particles in alkaline silica suspension, it is more convenient to develop a negative charge due to adhesion of silica species, which will later be attracted to the anode if quite high electric field strength is achieved. To verify this idea, we have performed the additional experiments seeking to determine the surface charge of hematite particles used in this study, although it is known that silica is a hydrophilic material with the negative surface charge over a wide pH range [33]. The method used was based on the idea that Fe_2O_3 particle surface becomes negatively charged by reacting with SiO_3^{2-} ions. The procedure of analysis was as follows: 0.5 g of Fe_2O_3 particles was agitated with 100 ml of potassium silicate solution for 1 h at room temperature. Then, the powder was centrifuged. The initial and final pH values of the solution were determined with a pH meter. When the Fe_2O_3 powder was added to the solution, its pH increased from 11 to 11.2.

From U_a vs t plots obtained in this study, it can be suggested that the deposition process starts after formation of a thin TiO_2 film because $U_a(t)$ plots in Fe_2O_3-containing and Fe_2O_3-free solutions attained within the first 7 to 10 s are close to approximately 70 V. Additionally, chemical state analysis of this film confirmed the formation of the TiO_2 film because the experimental value of the binding energy for Ti $2p_{2/3}$ peak in the XPS depth profiling studies equaled to 458.4±0.2 eV.

To gain insight into the reasons preventing a sharp voltage growth during galvanostatic anodizing in slurry solution, we performed SEM and XPS investigations of the Ti surface after the first 5, 10, 15, and 20 s of this process. In this setup, the top-down view of SEM images (Fig. 6) indicated the attachment of iron oxide corpuscles to the Ti surface just after onset of the anodic treatment. In addition, the contamination of Fe_2O_3 at approximately the same loading less than 1.0 at.% was confirmed by the XPS analysis. These results are in agreement with variables in the TiO_2 film color caused by the hematite particle inclusions in the titania film. During the first 4 s, the gray color of Ti anode, characteristic of TiO_2, remains the same and the bath voltage of about 55 V is attained. With further processing, the color of Ti surface changes to greenish, then yellow, sand finally red due to the incorporation of Fe_2O_3 particles in the titania layer. The spontaneous packing of Fe_2O_3 species, enveloped with SiO_3^{2-}, starts when a suitable electric field strength is reached.

Conclusions

Herein, we have demonstrated that a relatively thick coating mainly composed of α-Fe_2O_3 crystalline species and amorphous SiO_2 with the approximately 1:1 content ratio can be produced onto Ti anode by galvanostatic treatment in alkaline $K_2O{\cdot}SiO_2$ (molar ratio 1:3.1) suspension of Fe_2O_3 powder. The process of electrophoresis deposition starts just after the formation of the titania (TiO_2) layer with Fe_2O_3 particle inclusions distributed randomly throughout the film with approximately ≤1.0 at.% loading, preventing, however, a further bath voltage sharp growth and micro-arc phenomena typical of Fe_2O_3-free solution. The corresponding morphology of products was characterized by SEM and the composition of coatings by Mössbauer, EDX, XRD, and X-ray photoelectron spectroscopy. Based on these results, we suggest that Fe_2O_3 corpuscles in the solution of this study are enveloped with negatively charged SiO_3^{2-} ions and can migrate towards the anode and be attached to the substrate when the suitable electric field strength is reached.

The method reported herein for fabrication of the Fe_2O_3/SiO_2 composite coatings is simple and cheap, presenting nice opportunities for future technological applications. Further work is needed to determine how changes in the iron oxide particle size and phase composition would influence the final products which can be produced in such systems.

Acknowledgments This research was in part supported by a grant from the Lithuanian State Science and Studies Foundation (C-07035). The authors are grateful to Remigijus Juškėnas from the Institute of Chemistry for assistance in XRD spectroscopy.

References

1. Široky K, Jirešova J, Hudec LO (1994) Thin Solid Films 245:211. doi:10.1016/0040-6090(94)90902-4
2. Matijević E, Scheiner P (1978) J Colloid Interface Sci 63:509. doi:10.1016/S0021-9797(78)80011-3
3. Faust B, Hoffmann M, Bachnemann D (1989) J Phys Chem 93:6371. doi:10.1021/j100354a021

4. Gong C, Chen D, Jiao X, Wang Q (2002) J Mater Chem 12:1844. doi:10.1039/b201243j
5. Baltes M, Mathieu M, Vansant EF (2002) J Phys Chem B 106:13146. doi:10.1021/jp0211640
6. Park S, Lim S, Choi H (2006) Chem Mater 18:5150. doi:10.1021/cm0601990
7. Lee CW, Jung SS, Lee JS (2008) Mater Lett 62:561. doi:10.1016/j.matlet.2007.08.073
8. Zhang LY, Feng J, Xue DS (2007) Mater Lett 61:1363. doi:10.1016/j.matlet.2006.07.049
9. Gao CX, Liu QF, Xue DS (2002) J Mater Sci Lett 21:1781. doi:10.1023/A:1020941325311
10. Wang HW, Lin HC, Yeh YC, Kuo CH (2007) J Magn Magn Mater 310:2425. doi:10.1016/j.jmmm.2006.10.814
11. Suber L, Imperatori P, Ausanio G, Fabbri F, Hofmeister H (2005) J Phys Chem B 109:7103. doi:10.1021/jp045737f
12. Cornell RM, Schwertmann U (2003) The iron oxides, 2nd edn. Wiley-VCH, Weinheim
13. Kulkarni SS, Lokhande CD (2003) Mater Chem Phys 82:151. doi:10.1016/S0254-0584(03)00212-8
14. Choi KH, Lee SH, Kim YR, Malkinski L, Vovk A, Barnakov Y, Park JH, Jung YK, Jung JS (2007) J Magn Magn Mater 310:e861. doi:10.1016/j.jmmm.2006.11.022
15. Zou G, Xiong K, Jiang C, Li H, Li T, Du J, Qian Y (2005) J Phys Chem B 109:18356. doi:10.1021/jp052678c
16. Noorjahan M, Kumari VD, Subrahmanyam M, Boule P (2004) Appl Catal B 47:209. doi:10.1016/j.apcatb.2003.08.004
17. Sakthivel S, Shankar MV, Palanichamy M, Arabindoo B, Murugesan V (2002) J Photochem Photobiol A 148:153. doi:10.1016/S1010-6030(02)00085-0
18. Zhang RB (2005) J Non-Cryst Solids 351:2129. doi:10.1016/j.jnoncrysol.2005.04.048
19. Gao Y, Liu H (2005) Mater Chem Phys 92:604. doi:10.1016/j.matchemphys.2005.02.018
20. Geus JW (1986) Appl Catal 25:313. doi:10.1016/S0166-9834(00)81249-X
21. Huo L, Li W, Lu L, Cui H, Xi S, Wang J, Zhao B, Shen Y, Lu Z (2000) Chem Mater 12:790. doi:10.1021/cm990690+
22. Ohmori T, Takahashi H, Mametsuka H, Suzuki E (2000) Phys Chem Chem Phys 2:3519. doi:10.1039/b003977m
23. Catti M, Valerio G, Dovesi R (1995) Phys Rev B 51:7441. doi:10.1103/PhysRevB.51.7441
24. Hansen MF, Koch CB, Mørup S (2000) Phys Rev B 62:1124. doi:10.1103/PhysRevB.62.1124
25. Xu X, Wang J, Yang C, Wu H, Yang FJ (2009) Alloys Compd 468:414. doi:10.1016/j.jallcom.2008.01.013
26. Philipse AP, Bruggen MPB, Pathmamanoharan C (1994) Langmuir 10:92. doi:10.1021/la00013a014
27. Solinas S, Piccaluga G, Morales MP, Serna CJ (2001) Acta Mater 49:2805. doi:10.1016/S1359-6454(01)00160-4
28. Lu Y, Yin YD, Brian TM, Xia YN (2002) Nano Lett 2(3):183. doi:10.1021/nl015681q
29. Malyshev VN, Zorin KM (2007) Appl Surf Sci 254:1511. doi:10.1016/j.apsusc.2007.07.079
30. Wagner CD, Riggs WM, Davis LE, Moulder JF, Muilenberg GE (1978) Handbook of X-ray photoelectron spectroscopy. Perkin-Elmer, Minnesota
31. Patel MN, Williams RD, May RA, Uchida H, Stevenson KJ, Johnston KP (2008) Chem Mater 20:6029. doi:10.1021/cm8012705
32. Yerokhin AL, Nie X, Leyland A, Matthews A (2000) Surf Coat Technol 130:195. doi:10.1016/S0257-8972(00)00719-2
33. Somasundaran P (ed) (2006) Encyclopaedia of surface and colloid science. Taylor & Francis, New York, p 1857